Journal of Applied Physics

Electronic structure spectroscopy of organic semiconductors by energy resolved-electrochemical impedance spectroscopy (ER-EIS)

Cite as: J. Appl. Phys. **128**, 150902 (2020); https://doi.org/10.1063/5.0022289
Submitted: 29 July 2020 . Accepted: 02 October 2020 . Published Online: 20 October 2020

Franz Schauer

Journal of Applied Physics PERSPECTIVE scitation.org/journal/jap

Electronic structure spectroscopy of organic semiconductors by energy resolved-electrochemical impedance spectroscopy (ER-EIS)

Cite as: J. Appl. Phys. **128**, 150902 (2020); doi: 10.1063/5.0022289
Submitted: 29 July 2020 · Accepted: 2 October 2020 ·
Published Online: 20 October 2020

Franz Schauer[a)]

AFFILIATIONS

Faculty of Applied Informatics, Tomas Bata University in Zlin, 760 05 Zlin, Czech Republic

[a)]**Author to whom correspondence should be addressed:** fschauer@fai.utb.cz

ABSTRACT

Organic electronic applications are envisioned to address broad markets, which includes flexible displays, electronic papers, sensors, disposable and wearable electronics, and medical and biophysical applications, leading to a tremendous amount of interest from both academia and industry in the study of devices. These fields of science and technology constitute interdisciplinary fields that cover physics, chemistry, biology, and materials science, leading, as a wanted output, to the elucidation of physical and chemical properties, as well as structures, fabrication, and performance evaluation of devices and the creation of new knowledge underlying the operation of organic devices using new synthesized organic materials—organic semiconductors. We testify the situation when the available organic electronic applications sometimes lack a theoretical background. The cause may be the complicated properties of disordered, weak bounded, molecular materials with properties different from their inorganic counterparts. One of the basic information-rich resources is the electronic structure of organic semiconductors, elucidated by the methods, hardly possible to be transferred from the branch of inorganic semiconductors. Electrochemical spectroscopic methods, in general, and electrochemical impedance spectroscopy, in particular, tend and seem to fill this gap. In this Perspective article, the energy resolved-electrochemical impedance spectroscopic method for electronic structure studies of surface and bulk of organic semiconductors is presented, and its theoretical and implementation background is highlighted. To show the method's properties and strength, both as to the wide energy and excessive dynamic range, the basic measurements on polymeric materials and D–A blends are introduced, and to highlight its broad applicability, the results on polysilanes degradability, gap engineering of non-fullerene D–A blends, and electron structure spectroscopy of an inorganic nanocrystalline film are highlighted. In the outlook and perspective, the electrolyte/polymer interface will be studied in general and specifically devoted to the morphological, transport, and recombination properties of organic semiconductors and biophysical materials.

I. INTRODUCTION

A. Organic semiconductors

Research on organic electronic materials has thrived and expanded due to their promise to deliver applications with novel functionalities complementary to existing silicon technology. It is even possible that plastic electronics may replace silicon in applications that operate under modest performance requirements due to their reduced-complexity processing, compatibility with arbitrary substrates, and versatile chemistry. The seemingly infinite variety of organic compounds presents the prospect of tailoring materials to have any desired properties. Organic-based applications are envisioned to address a broad market, which includes flexible displays, electronic papers, sensors, disposable and wearable electronics, and medical and biophysical applications. Therefore, there is a tremendous amount of interest from both academia and industry in the study of devices such as organic field-effect transistors (OFETs), organic photovoltaics (OPVs), organic light-emitting diodes (OLEDs), and organic sensors.[1]

In recent years, new fields of organic electronics, organic optoelectronics, and organic photonics using organic materials have opened up, paved by the work of numerous laboratories and Nobel prize winners in the field.[2] These fields of science and technology, which are mostly related to information and energy, are mainly concerned with thin-film, flexible devices using organic materials, constituting interdisciplinary fields that cover physics, chemistry, biology, and materials science. The science and technology of these fields, which can be termed organic functional materials science or organic device science, include wide areas from the molecular design and synthesis of photoactive and electroactive organic materials to the elucidation of their physical and chemical properties, as well as their structures, fabrication, and performance evaluation of devices and the creation of new knowledge underlying the operation of organic devices using new synthesized organic materials—organic semiconductors (OS).[3]

Organic semiconductors, amorphous molecular films, molecular crystals, and the polymer film differ from their inorganic counterparts by extrinsic conductivity, resulting from the injection of charges at electrodes, from intentional or unintentional doping and from the dissociation of photogenerated electron–hole pairs that are bound by their mutual Coulomb attraction. Organic semiconductors possess two major characteristic features influencing deeply their properties—first, absorption and emission take place in the range of 600–400 nm, which precludes creating any significant charge-carrier concentration by thermal excitation at room temperature; second, the low permittivity implies that Coulomb interactions are significant so that any electron–hole pair created by optical excitation is bound by strong coulomb energy. The overwhelming majority of textbooks on semiconductor devices are concerned with inorganic semiconductors, and, as a consequence, concepts originally developed to explain photophysical processes in crystalline inorganic semiconductor devices are sometimes employed to account for the operation of devices made with amorphous organic semiconductors. In most cases, this does not work. One may conclude that the underlying physics of organic semiconductors is very different from that of their inorganic analogs. This is not the case. The laws of physics are very same ones, yet some parameters take on different values (Ref. 4, p. 171). Also, the fact that in amorphous organic semiconductors the charge-transporting moieties are coupled by weak van der Waals force has two important consequences: first, when abandoning the crystallographic order in molecular crystal, no bond breaking occurs, that is, there are no dangling bonds; second, valence and conduction bands are completely decomposed into a manifold of localized state and charge carriers hop randomly between the structural elements (Ref. 4, p. 175).

The background of the electrochemical systems with disordered organic semiconductors is rather complicated, lying at the border of electrochemistry and solid-state physics, encompassing transport of several types of species charged and neutral, ionic and electronic, with rather different properties as ions intercalation and pore structure, deteriorating conductive polymer (CP) structure and properties. All these circumstances make also the branch of electrochemical spectroscopic systems with disordered organic semiconductors rather demanding.

Current and near-future applications and information[4,5] and future trajectory of organic electronics[6] are to be found in recent materials.

B. Electronic structure of organic semiconductors

Organic semiconductors may be divided into three groups: molecular crystals, amorphous molecular films, and polymer films. Semiconductor properties in all types of organic semiconductors have a similar origin: the energy levels of the prevailing π electrons. Polymeric films, in the molecular-based case approach, may be considered a polymeric chain, as a sequence of molecular repeat units such as alternating single and double bonds coupled with covalent bonding. As a result of coupling, the orbitals of adjacent units interact and split. This process takes across the entire chain leading to the formation of bands. Thus, π and π* bands arise, and they take the role of a valence and conduction band. A critical quantity, however, is the relative size of the coupling energy between the repeat unit compared to the energetic variation of each unit (Ref. 4, pp. 176–177).

In an amorphous polymeric film, an energetic disorder due to the polarization of the surroundings is strong, so that electronic coherence is only maintained over a few repeat units, that is, the conjugated segment. Accidental or deliberate doping leading to reduction or oxidation, as well as charge injection or exciton dissociation, creates charged chromophores. The chromophores may be entire molecules or conjugated segments of a polymer chain. The electronic structure of disordered organic solids is used, in connection with neutral and charged states, to explain on the microscopic level the charge transport, trapping, and recombination using the Gaussian disorder model, also known as the Bässler model.[7] It is based upon the notion that charge carriers hop within a manifold of sites that feature a Gaussian energy distribution and Gaussian distribution of inter-site spacing.

The energy levels of molecules are described by Gaussian distribution as

$$g(E) = \frac{1}{\sqrt{2\pi\sigma}}\, e^{\left[\frac{-(E-E_0)^2}{2\sigma^2}\right]},$$

where E is the energy of an individual molecule, and the standard deviation σ (as a disorder parameter) characterizes the width of the Gaussian distribution. The distribution results mainly from the van der Waals coupling with the neighboring sites and due to the variation in the length of conjugated elements of the polymer chain. An equivalent to the valence and conduction bands in inorganic solids emerges HOMO and LUMO as the highest occupied and lowest unoccupied molecular orbitals, respectively. Due to the low dielectric constant and electron–electron interaction, when charge carriers are transported, the molecule will adapt to the (single) positive or the negative charge in the HOMO or LUMO level, respectively, resulting in positive or negative polaronic hopping transport levels (in contrast to the delocalized bands in inorganic semiconductors). They are separated by the transport gap, also called the single-particle gap (Fig. 1).

The electronic structure of intrinsic and extrinsic defects in organic semiconductors is a major topic of organic electronics. The former arises from the morphological disorder inherent in the amorphous nature of a typical organic film and the latter stems from extrinsic defects, such as chemical impurities introduced during material synthesis, device fabrication or exposure to oxygen or moisture, and an electrochemical process involving oxygen. The

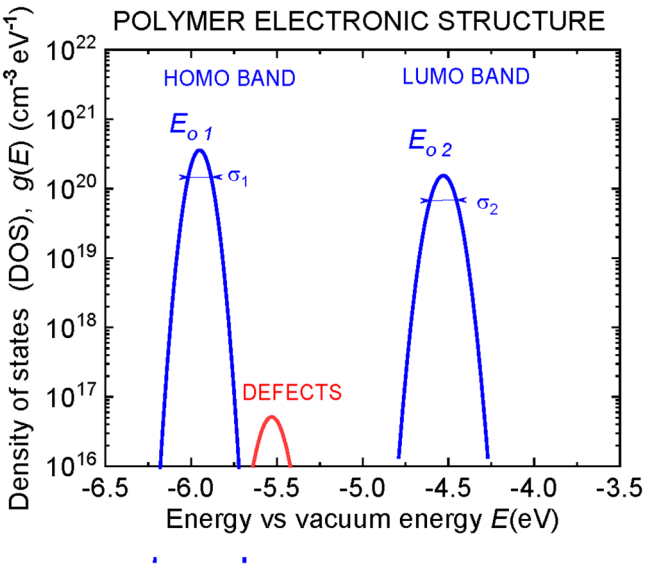

FIG. 1. Schematic diagram of the electronic structure with the HOMO, LUMO, and DEFECTS bands.

nature of these induced defects, their energy state distribution, the physical and chemical mechanisms of their creation and creation kinetics, and their relation to native defects are important problems. In any microelectronic device, fundamental physical parameters including the electron structure of defects must be well understood for successful electronic optimization.[8]

C. Electronic structure methods

Determination of the electronic structure of organic semiconductors has major relevance for studies of charge/energy transport and recombination phenomena in organic electronics. The major differences between organic and inorganic semiconductors demonstrate that detailed knowledge on the electronic structure is needed to understand their photophysical properties, and even more if one wishes to design and improve the semiconductor device. However, weak molecular coupling and disordered structures often preclude the application of the spectroscopic methods used for inorganic semiconductors (Ref. 4, p.171). In principle, for studying the electronic structure of organic semiconductors, the following methods are suitable: capacitance methods,[9] sub-bandgap photoconductivity,[10] photoelectron spectroscopies UPS (Ultraviolet Photoelectron Spectroscopy) and IPES (Inverse Photoelectron Spectroscopy),[11] and electrochemical methods.[12,13]

For studying the electronic structure of defect states in organic semiconductors, several methods were accommodated for the elucidation of defects: thermally stimulated current (TSC), fractional thermally stimulated current (FTSC), space charge limited (SCL) current, capacitance vs voltage (CV), capacitance vs frequency (CF), and drive-level transient spectroscopy (DLTS) (see details in Ref. 14).

There is a gap in existing methods for studying the exclusive electronic structure of organic semiconductors. It is desirable to have a method, providing information concerning the electronic structure of progressive blend systems with organic semiconductors, as depicted schematically in Fig. 2 (left) and the result of electronic structure spectroscopy in Fig. 2 (right). Electrochemical spectroscopic methods, in general, and electrochemical impedance spectroscopy, in particular, tend to fill this gap, as explained next.

D. Electrochemical methods

Electrochemical Impedance Spectroscopy (EIS) has been known for decades and has served many purposes, from studies of electrochemical reaction mechanisms to investigations of passive surfaces. EIS development has also been positively influenced by the activities related to clarification of solid-electrolyte processes over the last 40–50 years.[15]

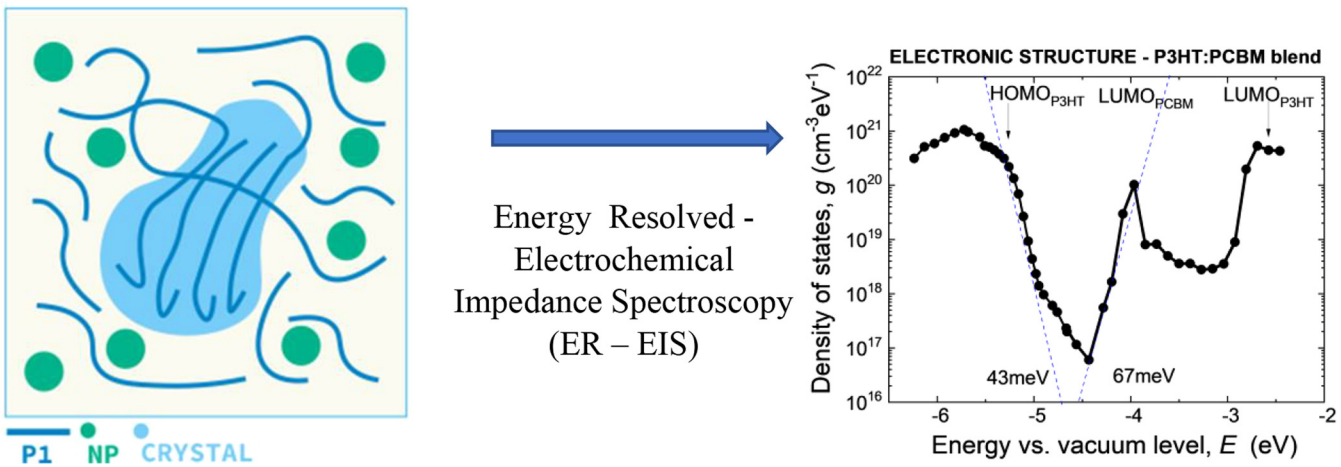

FIG. 2. Schematic representation of the blend system of donor polymer (P1), acceptor nanoparticle (NP), and polymer crystallite (CRYSTAL) (left) and electronic structure (here P3HT: PCBM, measured by ER-EIS method) (right).

A new dimension in using electrochemical methods for studying the electronic structure of organic semiconductors offers the concept of the Helmholtz double-layer (HDL) formed at the interface of an electrolyte/OS by the controlled density of ions (anions and cations) in the electrolyte and by equal, but opposite charge surface density, of electronic charge carriers in the semiconductor.[16,17] The ions and electronic charge carriers screen in equilibrium more or less completely the electric field outside HDL. Because the distance between ions and electronic charge carriers ranges from 1 to 10 nm, internal electric field strength results in the range of $1–10 \times 10^6$ V cm^{-1} with a charge-carrier density of the order of 10^{13} cm^{-2}.[18] For using the HDL in the study of organic semiconductors, various charge-transfer processes must be recognized both at the interface and in the bulk of OS. The field is the basis of chemical reactions, cultivated from the 50th of 20th century by Marcus, who elaborated successively the general theory of electronic transfer,[19] liquid/liquid interfaces,[20] and electrolyte/solid-state materials with delocalized transport, as are electrolyte/metal interfaces[21] and inorganic crystalline semiconductors with diffusion-limited process and the overall bimolecular rate of the diffusion-limited process $k_{ept-} = 10^{-17}–10^{-18}$ cm^4 s^{-1}.[22] Many theoretical and experimental works followed, proving the theory of Marcus, with barrier-breaking papers on glassy organic molecular materials by Miller,[23] electrolyte/graphite electrodes,[24] and electrolyte/molecular spacers and wires.[25]

The occurrence of OS with electronic transport, followed by an overwhelming range of applications, left the field with many unsolved problems, both in electrochemistry and in solid-state physics. Several groups made progress in interface charge transport in the electrolyte.[26–28] Two excellent papers dealing with the electronic structure of semiconductor nanoparticles occurred.[29,30]

Heterogeneous interface electrolyte/OS constitutes a multistep reaction in the environment electrolyte/solid electrode. Its basis is the branch of chemical reactions present in various environments encompassing reactions in chemistry via biology to biophysics.[31,32] Charge-carrier in heterogeneous D–A (or A–D) reaction, from the solvated ion as a donor D to charged acceptor A as a scavenger in OS, is governed by the slowest hopping step in OS by many orders of magnitude,[33] and, thus, hopping transport cannot be properly inserted in the diffusion-limited transport framework. The contemporary models of de Vries *et al.*[34] do not provide closed solutions to be inserted into semiclassical Marcus models. This is the reason for embarking on the outlining of the consequences of the sluggish transport in an OS and finding the pre-exponential term for the transport in OS only. Already the first works on electrolyte/redox polymers, albeit very limited, indicated and foresaw the peculiarities with the predominant reaction-limited (in contrast to diffusion-limited) type of transport in the electrolyte/OS systems.[35,36]

The spectroscopic method of Energy Resolved-Electrochemical Impedance Spectroscopy (ER-EIS) for the elucidation of the electronic structure of OS published in 2014 (and preliminary results in 2013) is described below.[37]

II. ER-EIS SPECTROSCOPY

A. ER-EIS method principle

If an OS is immersed in the electrolyte with the negatively biased Pt electrode, with respect to the OS ($V_{Pt} < 0$), the HDL is established, formed by the negative salt ions in the redox electrolyte and positively charged surface of the HOMO states of the OS with density p_{surf}. In Fig. 3(a), the detail of the charge transfer at the surface of OS is depicted. [Note: In the case of the positively biased electrode, with respect of OS ($V_{Pt} > 0$), HDL with a negatively charged surface of the LUMO states of OS with density n_{surf} occurs and spectroscopy of LUMO states is possible; for simplicity, we will describe the former case with HOMO charged states throughout this paper, and application to LUMO states is straightforward.] If the Pt electrode and the OS sample form a closed circuit, the surface concentration of positive holes is neutralized (reduced) by electrons incoming from the electrolyte by diffusion, forming recombination current j_{rec} [carrying the first of the spectroscopic information of the method ER-EIS; see Eqs. (A5) and (A6)] and establishing the Fermi energy E_{Fp} in OS.[38,39] We will denote in Eq. (A5) the product $k_{eteff} = k_{et}(E)V_f$ as the effective bimolecular electronic transfer rate, where V_f is the volume fraction of electrons in 1 cm^3 that are able to participate in the transfer reaction, determined by the effective coupling length of the acceptor species in the semiconductor electrode. It has been estimated that adiabatic charge transfer can occur for species up to 1 nm from the electrode surface, and thus $V_f \approx 10^{-7}$ (Refs. 40 and 41) and $k_{et}(E)$ is the bimolecular electronic transfer rate. To support the steady-state current in the bulk of the OS, the electric field strength in the bulk of the OS, followed by the injection of holes from the back (rear) contact of OS, forms the current in the OS bulk, $j_{bulk} = j_{rec.}$

The majority of pertinent literature deals with the systems' electrolyte/metal or electrolyte/poly (or nano) crystalline semiconductors[42,43] based on the Marcus theory,[22] not touching the electrolyte/OS system. It may be caused by the differences the system electrolyte/disordered OS represents, which may be summarized as follows:[46] (1) the homogeneous thin OS layer, prepared under the optimized conditions with the clean surface without any adsorbed species, kept in a protective atmosphere (glovebox) during both preparation and experiment and the absence of any inhomogeneous structures. (The influence of pores in OS on the spectroscopic results of ER-EIS results will be discussed in the subsequent paper.) OSs for organic electronics are intentionally produced with a negligible apparent Brunauer–Emmett–Teller (BET) surface area of less than 50 m^2 g^{-1};[44] (2) charge transport by hopping with a defined transport path; (3) the bulk of the polymer, characterized by the continuous DOS function $g(E)$ of hopping sites; and (4) supposing, along with Salaneck *et al.*,[45] the surface electronic structure of polymers is well represented by that of the bulk, in other words, there are no surface states in OS.

In discussing the OS bulk charge transport in the system electrolyte/OS, several circumstances have to be taken into consideration. The interface electrolyte/OS absorbs majority of the applied external voltage and induces current j_{bulk} in the bulk of OS and the Fermi energy E_{Fp} in the continuum of electron states of the HOMO of the OS with DOS filled up to E_{Fp}.[46]

This is the major difference from inorganic crystalline semiconductor electrodes, where the majority of the applied voltage is absorbed by the semiconductor, causing depletion or accumulation and the charge-carriers for the redox processes come from the conduction (valence) band edges, precluding semiconductor electron structure elucidation. Next, there is also problem in the value of the

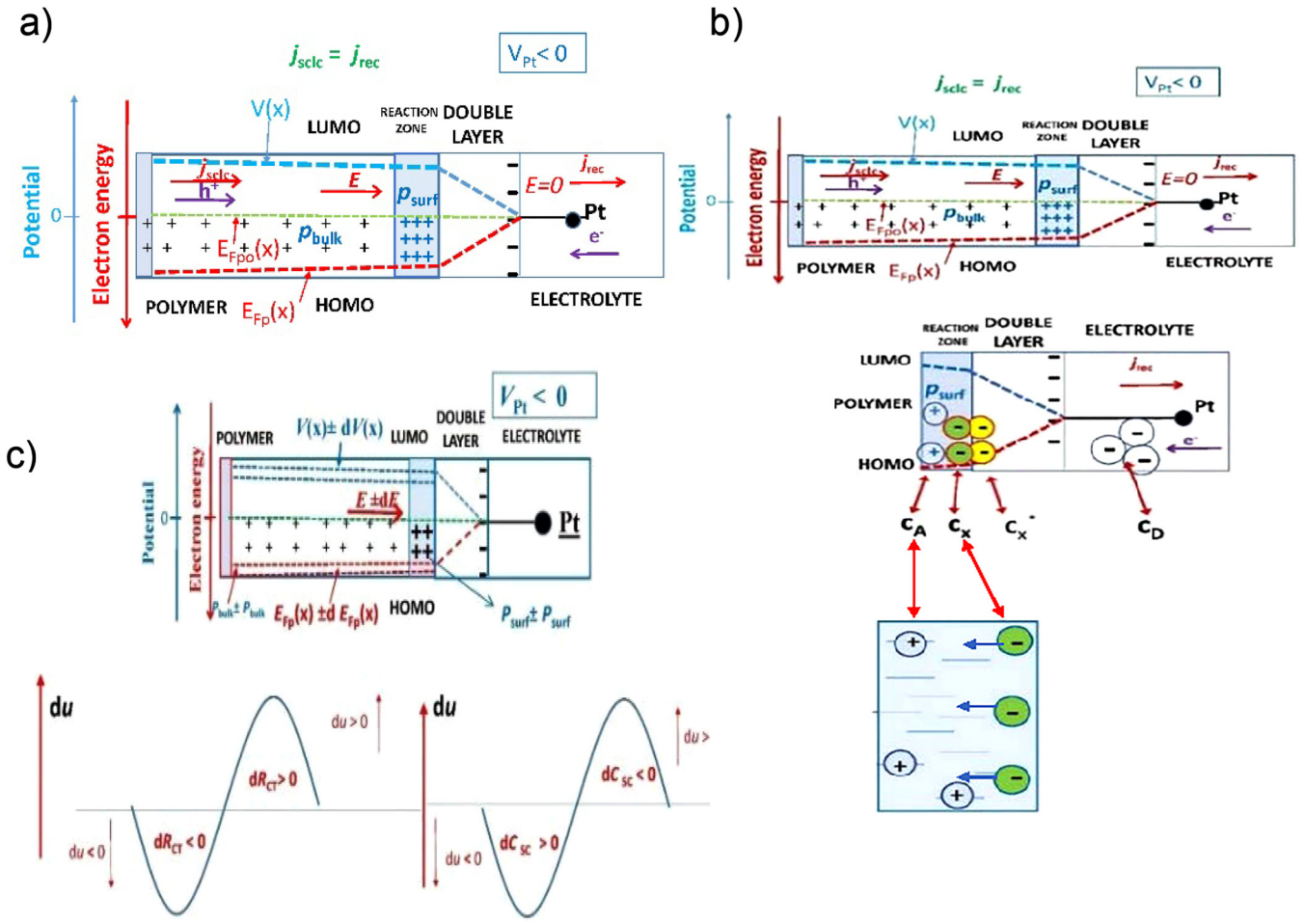

FIG. 3. The steady-state charge transport via interface electrolyte/organic semiconductor: (a) HDL and recombination current j_{rec} and bulk SCLC current j_{SCLC}, (b) detail of the charge-transfer at the surface of OS and the volume fraction of electrons in 1 cm^3 able to participate in transfer reaction, determined by the effective coupling length of the acceptor species in the semiconductor, and (c) the spectroscopic character of the method ER-EIS based on the measured phase-resolved impedance of the electrolyte/OS system $Z = R_{ct} + 1/j\omega C_{sc}$, where R_{ct} is the differential charge-transfer resistance, C_{sc} is the differential space–charge capacitance, and ω is the angular frequency.

maximum necessary bulk current densities, in the extremities of the HOMO with $g(E) \approx 10^{21}\ cm^{-3}\ eV^{-1}$ (Ref. 47) and the corresponding current densities of fractions of 1 A cm^{-2} and more. Such excessive values cannot be supported by common mechanisms of charge transport in the disordered OS, except for the Space–Charge Limited Currents (SCLC).[48,49] For the occurrence of SCLC, two basic conditions have to be fulfilled—the existence of the hole-injecting and extracting contact and electric field strength in the OS bulk. Compensating holes are injected from the back (rear) electrode forming the (SCLC) $j_{SCLC} = \frac{9}{8}\frac{\varepsilon\varepsilon_o\mu_o\Theta(U_{os})U_{os}^2}{L^3}$.[48] Here, U_{os} is the voltage at the OS ($U_{os} \approx 0$ V), $\epsilon\epsilon_o$ is the permittivity, σ is the electric conductivity, L is the thickness of the OS layer, and $\mu_d = \mu_o\,\Theta\,(U_{os})$ is the effective drift mobility, where μ_o is the mobility at the transport path and $\Theta(U)$ is the quotient of the electrons participating in the charge transport to all electrons in the system (mobile by hopping to all electrons, including those in deep traps). Injected charges (holes) may not be neutralized during the transit time and are forming space–charge (SC) q_{sc} per unit volume in the bulk of the OS [carrying the second independent spectroscopic information of the method ER-EIS; see Eqs. (A3) and (A4)].[50] The spectroscopic character of the method ER-EIS is based on the measured phase-resolved impedance of the electrolyte/OS system [see Fig. 3(c) $Z = R_{ct} + 1/j\omega C_{sc}$, where R_{ct} is the differential charge-transfer resistance, defined by Eq. (A6) and C_{sc} is the differential space–charge capacitance, defined by Eq. (A4), both as a response to a small perturbation harmonic voltage $\Delta U \sin(\omega t)$, where $\omega = 2\pi f$ (f is the frequency). The instantaneous position of the Fermi level E_{Fp} is adjusted by the externally applied voltage ramp, $E_{Fp} = eU$. Shifting the Fermi energy E_{Fp}, we obtain information on DOS functions via quantities $R_{ct}(E_{Fp})$ and $C_{sc}(E_{Fp})$. Important point

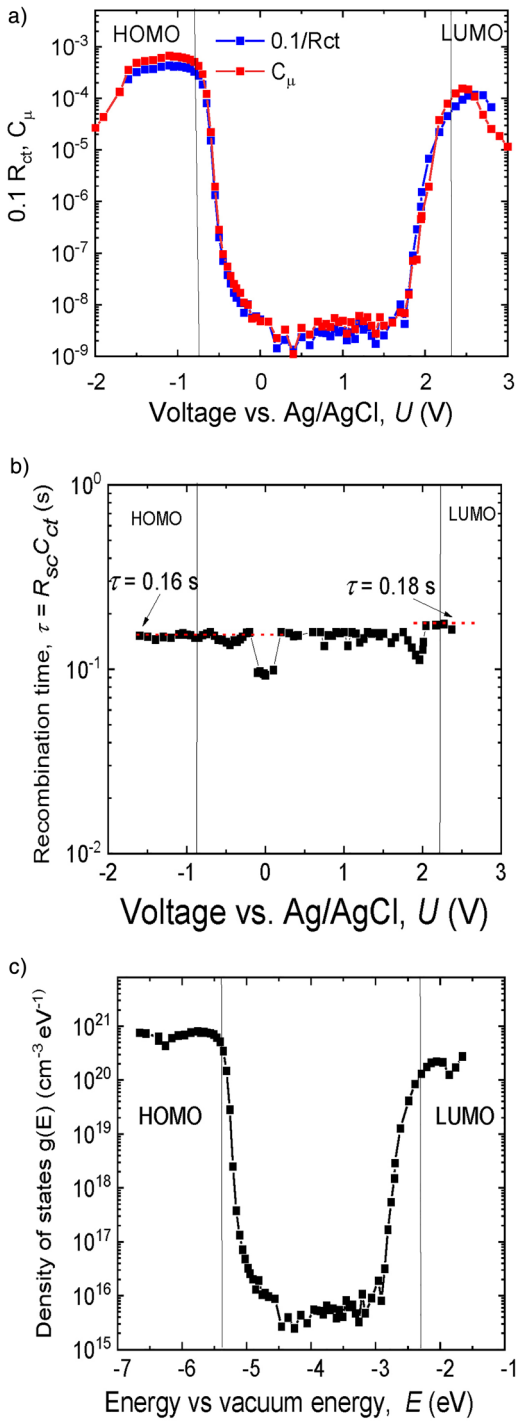

FIG. 4. ER-EIS spectra of P3HT films: (a) An example of rough unprocessed ER-EIS data plotted as $0.1/R_{ct}$ and C_{sc} vs applied voltage U with respect to the reference electrode Ag and AgCl, (b) the product of R_{ct} and C_{sc} for the calculation of the coefficient $k_{ct\ eff} = 3.12 \times 10^{-24}$ cm^4 s^{-1} [Eq. (A8)], and (c) the final surface DOS function $g(E)$ [Eq. (A6)].

worth stressing is that both quantities $R_{ct}(E_{Fp})$ and $C_{sc}(E_{Fp})$, provide an independent information on the electron structure of OS, the former of about nm thickness of the OS surface [see Figs. 3(b) and 3(c)] giving surface DOS $g_{ct}(E_{Fp})$ [Eq. (A6)] and the latter giving bulk DOS $g_{sc}(E_{Fp})$ [Eq. (A3)]. The experiment ER-EIS itself is relatively simple; the analyzer is connected in three-electrode configurations placed in a glovebox using a standard impedance/gain-phase regime. In Fig. 4(a), the example of rough unprocessed ER-EIS data on the P3HT film plotted as $0.1/R_{ct}$ and C_{sc} vs applied voltage U with respect to the reference electrode Ag–AgCl. In Fig. 4(b), the product of R_{ct} and C_{sc} for the calculation of coefficient $k_{ct\ eff} = 3.12 \times 10^{-24}$ cm^4 s^{-1} [Eq. (A8)] is provided, and, in Fig. 4(c), the final surface DOS function of $g(E)$ [Eq. (A6)] is provided.

B. EIS data—To obtain and process

The method EIS in its classical form provides rich information on any examined object.[51,52] In majority of the cases, the starting point of any reasoning about EIS results rests in the Equivalent Circuit (EC) of the examined object, either lumped or space-distributed.

The most used is the Randles EC[53] [see Fig. 5(a)], with electrolyte resistance R_s (possible to subtract from the measurement data), electrolyte/solid electrode HDL capacitance C_μ, recombination resistance R_{ct}, Wartburg impedance W, electrode bulk capacitance C_b, and transport bulk resistance R_t.

The goal of the EIS method is to extract from a wide frequency range measurements of complex impedance $Z(\omega)$, the sought components of EC. With the system electrolyte/OS, we aim at the components R_{ct} and $C_b = C_{sc}$, where it is $C_{sc} \gg C_{dl}$ and $R_t \gg 1/\omega C_{sc}$. Then, for low enough frequency, where $1/(\omega C_{dl}) \gg R_{ct}$, the EC simplifies to that depicted in Fig. 5(b), whose schematic Nyquist diagram is in Fig. 5(c). In Fig. 5(d), the EIS data for the P3HT film for three overvoltages $U = -0.3$, -0.5, and -1 V (scanning HOMO of CP) are provided. The dependences are probably influenced by the constant phase Wartburg term, and the differences from the ideal plot are small when plotted in log scale. The painstaking search for the optimal ER-EIS measuring frequency ω is, thus, not necessary. Another asset of the simplified EC for the system electrolyte/OS is shown in Fig. 5(e), depicting a schematic Nyquist diagram for variable overvoltage U and constant measuring frequency, resulting in a constant phase shift of impedance tg $\varphi = 1/(R_{ct}\,\omega C_{sc})$. In Fig. 5(f), the corresponding dependencies for the P3HT film of the real (showing $Z_{re} = R_{ct}$) and imaginary [showing $Z_{im} = 1/(\omega C_{sc})$] parts of the impedance (for frequency $f = 0.5$ Hz) on the overvoltage both for injection of holes in HOMO (left) and also electrons in LUMO (right).

In Fig. 6, both surface and bulk features of ER-EIS spectroscopy are highlighted. The rough ER-EIS data of P3HT $C_{sc}(E_{Fp})$ (red curve) and $R_{ct}(E_{Fp})$ (blue curve) are in Fig. 6(a). To obtain DOS bulk function of OS, $g_{sc}(E)$, we use a simple transformation [Eq. (A3)], with the result depicted in Fig. 6(b) (red curve). To obtain the DOS function of the OS surface, $g_{ct}(E)$, we use for transformation Eq. (A6) with the result depicted in Fig. 6(b) (blue curve). Both dependencies $g_{sc}(E)$ and $g_{ct}(E)$ exhibit similar waveforms, except for the surface feature in dependence $g_{ct}(E)$ peaking at energy -0.15 eV corresponding to crystallites in P3HT.

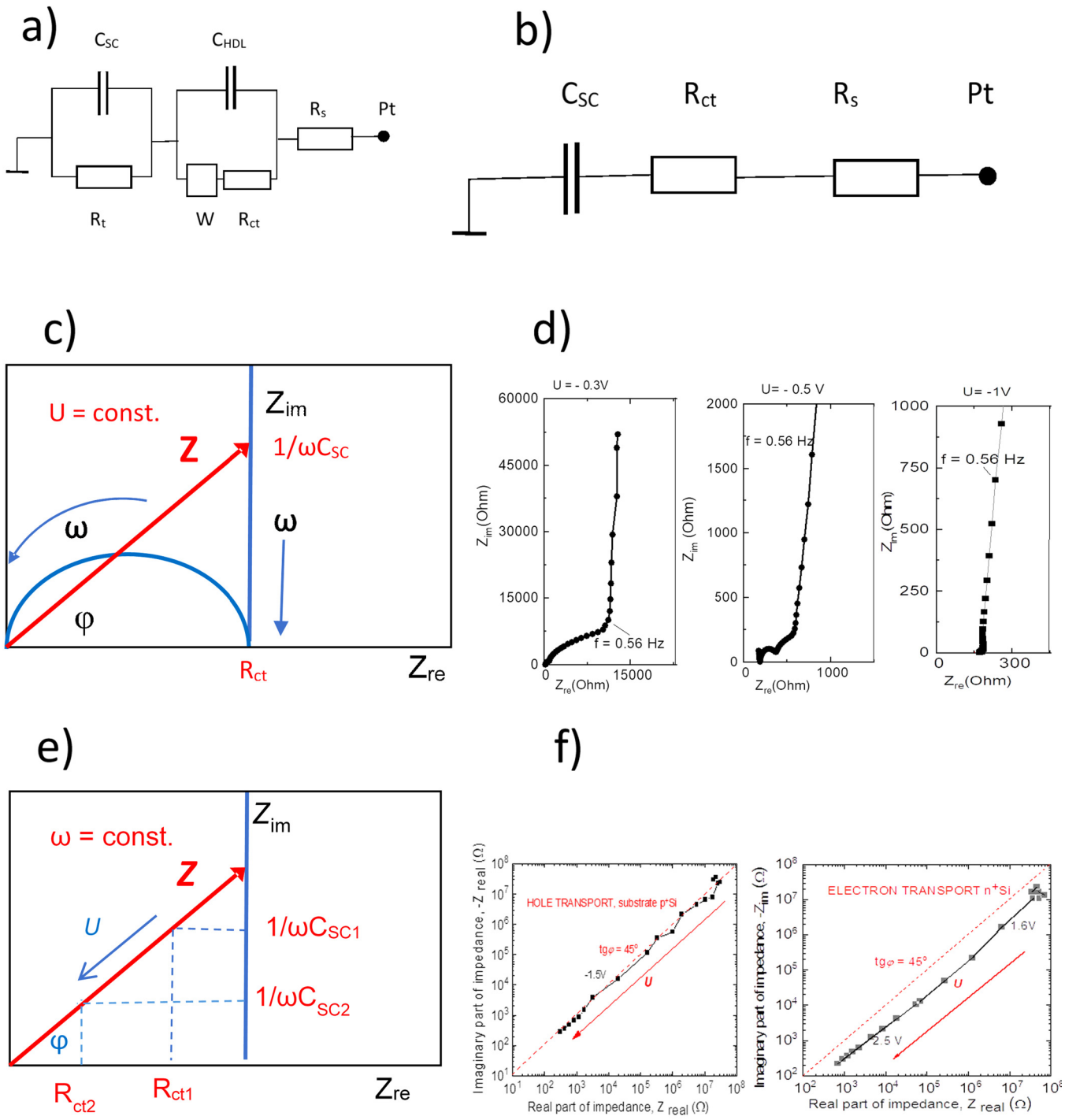

FIG. 5. Simplifying conditions for ER-EIS and system electrolyte/CP: (a) Randles equivalent circuit, (b) simplified equivalent circuit for the system electrolyte/CP, (c) the schematic Nyquist diagram for constant voltage U, (d) the EIS data for P3HT films for overvoltages $U = -0{,}3$, 0.5, and -1 V, (e) the schematic Nyquist diagram for constant frequency ω, and (f) the corresponding dependences for the P3HT film of the real (showing $Z_{re} = R_{ct}$) and imaginary (showing $Zim = 1/(\omega Csc)$ parts of the impedance (for frequency $f = 0.5$ Hz) on the overvoltage for both injection of holes in HOMO (left) and electrons in LUMO (right). Adapted from Schauer *et al.*, J. Appl. Phys. **124**, 165702 (2018).[57]

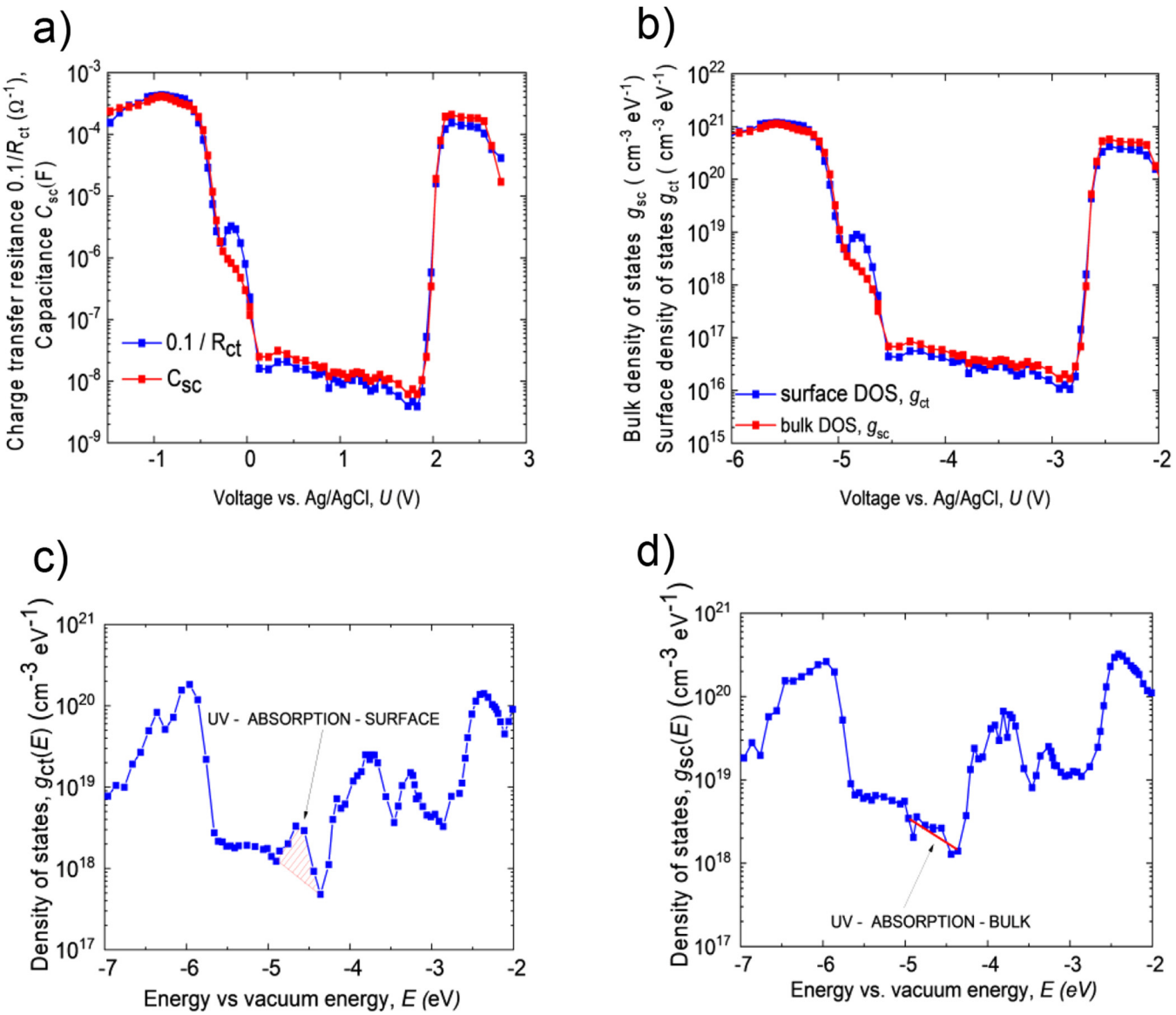

FIG. 6. Comparison of surface vs bulk DOS results of ER-EIS for the P3HT film: (a) The rough data of ER-EIS C_{sc} (E_{Fp}) (red curve) and R_{ct} (E_{Fp}) (blue curve) and (b) DOS bulk function of the OS, $g_{sc}(E)$ [Eq. (A3) (red curve)], DOS function of the OS surface, $g_{ct}(E)$ [Eq. (A6) (blue curve)]. Both dependencies $g_{sc}(E)$ and $g_{ct}(E)$ exhibit similar cause with exception of the surface feature in dependence $g_{ct}(E)$ peaking at energy −0.15 eV corresponding to crystallites in P3HT at the film surface. Comparison of surface vs bulk DOS results of ER-EIS for the MeLPPP-PCBM blend film illuminated by a UV laser diode (290 nm): (c) surface $g_{ct}(E)$ DOS and (d) bulk $g_{sc}(E)$ DOS (see text for details).

Differences in surface and bulk DOS functions were observed also MeLPPP-PC61BM 1:1 blend with expressed HOMO and LUMO (−5.88 and −4.15 eV) illuminated with the UV laser diode (290 nm). Figure 6(c) depicts surface DOS $g_{ct}(E)$, whereas Fig. 6(d) gives bulk DOS $g_{sc}(E)$. The signature of probably charge-transfer state (CT) at about −4.5 eV is visible only on the surface DOS function $g_{sc}(E)$ [Fig. 6(c)] due to the surface absorption of UV. Both experiments in Fig. 6 testify the mapping surface vs bulk ability of the ER-EIS method.[56]

III. APPLICATIONS OF ER-EIS SPECTROSCOPIC METHOD

To show possibilities of the method ER-EIS, let us show examples of published results with great application impact, summarized

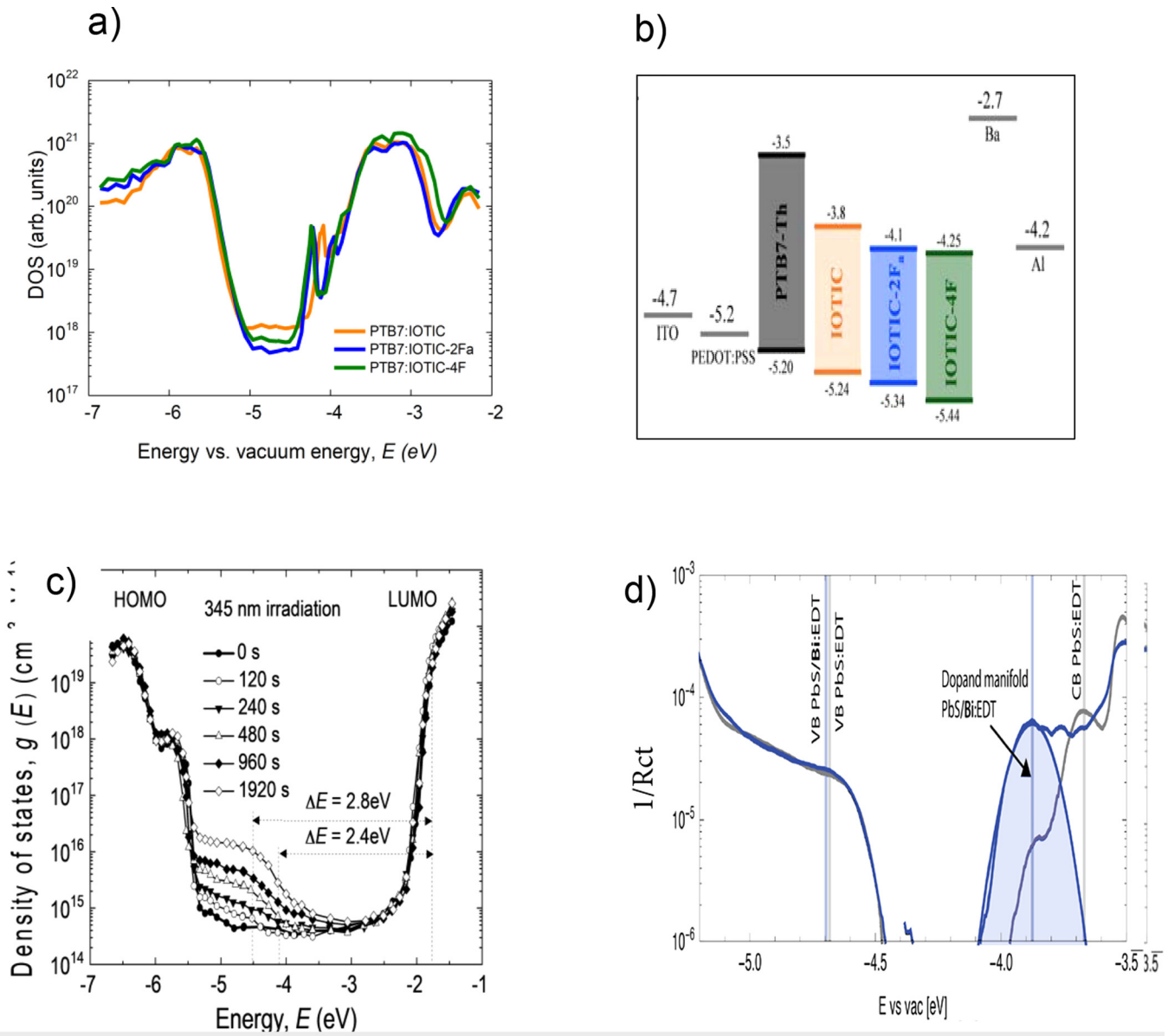

FIG. 7. Applications of the method ER-EIS: (a) The results of ER-EIS spectroscopy and gap engineering of the organic solar cell system with non-fullerene acceptors PTB7:IOTIC, PTB7:IOTIC-2Fa, and PTB7:IOTIC-4F, (b) the corresponding gap engineering results, (c) the results of ER-EIS spectroscopy on a wide bandgap silicon-based polysilane, PMPSi, and its degradation spectra by the UV laser (345 nm), correlated with the photoluminescence (PL) spectra in corresponding energy regions, and (d) ER-EIS results on PbS nanocrystal thin films. The necessary passivation of nanoparticle surface states, excluding obviously Fermi energy pinning, and calibrating of the method, was achieved. (a) and (b) Adapted from Karki *et al.*, Adv. Energy Mater. **10**, 2001203 (2020).[54] (c) Adapted from Schauer *et al.*, Polym. Degrad. Stability **126**, 204–208 (2016).[55] (d) Adapted from Volk *et al.*, J. Phys. Chem. Lett. **9**, 1384–1392 (2018).[30]

in Figs. 7(a)–7(d). In Fig. 7(a), the results of ER-EIS spectroscopy and of gap engineering [Fig. 7(b)] on the organic solar cell system with non-fullerene acceptors PTB7:IOTIC, PTB7:IOTIC-2Fa, and PTB7:IOTIC-4F are provided. The excessive resolving power and dynamics of ER-EIS are obvious.

In Fig. 7(c), ER-EIS results for silicon-based polysilanes, PMPSi, and its degradation results by UV radiation (345 nm), correlated with the measured photoluminescence (PL) spectra in corresponding energy regions 2.8 and 2.4 eV, are provided.[55]

In Fig. 7(d), very encouraging results of ER-EIS on PbS nanocrystal thin films are provided.[30] Surprising is the use of the method ER-EIS on the inorganic crystalline material, where the passivation of nanoparticles surface states, excluding obviously the Fermi energy pinning and calibrating the DOS output of the method, was the main result.

IV. OUTLOOK AND CONCLUDING REMARCS

Examination of the phenomena at the interface electrolyte/OS brings much information of the organic semiconductor. Surprisingly, the critical structure–property relationships in the electrochemical systems are still few in number relative to the synthetic knowledge found in solid-state organic electronics. In particular, key structure–property relationships to control electron transfer reactions between CP backbones and redox species within an electrolyte have received significantly less attention than the hybrid electronic–ionic conduction mechanism, despite the two processes being closely connected. Let us mention a few to deal with in connection with the ER-EIS method: The found range of the bimolecular recombination coefficients k_{ct} via the ER-EIS method for various organic semiconductors and their systems [$k_{ct} = (1–10)\ 10^{-24}\ cm^4\ s^{-1}$] seem to indicate k_{ct} to be the figure of merit for the comparison of different material systems and may express the properties of both the surface and bulk of the organic semiconductor:[27]

- The determination of the electronic structure of an organic semiconductor by ER-EIS has major relevance for studies of charge and energy transport and recombination phenomena in organic electronics both in the dark and the excited states. The method may be with advantage used for the study of percolation transport in D–A blends.
- The morphology and pore structure tell decisively on the electronic structure with organic semiconductor, and, thus, the ER-EIS method may be used as the method for their study.
- The study by ER-EIS of the charge transfer at the surface of OS and the volume fraction of electrons in $1\ cm^3$ able to participate in the transfer reaction, determined by the effective coupling length of the acceptor species in the semiconductor of about 1 nm.
- The system electrolyte/OS showed the way how to provide OS with barrier-less injection and extraction contacts, leading to the high achieved current up to $\approx 1\ A\ cm^{-2}$, electric conductivity up to $\approx 10^5\ \Omega^{-1}\ cm^{-1}$, and accumulated charge densities up to $\approx 10^2\ C\ cm^{-3}$ in the ER-EIS method indicate its high applicational potential in the molecular electronics.

In conclusion, we may summarize the electrochemical ER-EIS method, with success, used for measuring the electronic structure of organic semiconductors and their blends and study their properties with all advantages the electrolyte/OS contact possesses for the barrierless charge transport.

This Perspective article intends to show a new method for the elucidation of electron structure of organic semiconductors and filling the gap through the unconventional electrochemical spectroscopical method. The authors' hope is to facilitate understanding and background of the subject matter of the new spectroscopical method and to help its wide dissemination.

ACKNOWLEDGMENTS

The author thanks the Editor-in-Chief of *Journal of Applied Physics*, Dr. Andre Anders, for the nomination and invitation to submit this Perspective. The author is deeply grateful for the friendly comments and help of Professor H. Bäessler, Professor A. Köhler, and Professor S. Nešpůrek. At the same time, the fruitful discussions and cooperation during the ER-EIS method building and optimizing with Dr. K. Gmucová and Dr. V. Nádaždy is acknowledged. Thanks also goes to postdoctoral and doctoral students Dr. T. Váry, Dr. L. Tkáč, and M. Tkáčová for an extended and time-consuming experimental help in the data collection. The author is also grateful for the help of several doctoral students of Tomas Bata University in Zlin, M. Krbecek, M. Gerza, and P. Beňo.

APPENDIX: ER-EIS EVALUATION IN A NUTSHELL

The measured quantity is the phase-resolved impedance,

$$Z = Z_{re} + jZ_{im} = R_{ct}(E_F) + j\frac{1}{\omega C_{sc}(E_F)} \quad (E_F = eU). \tag{A1}$$

1. Bulk of conductive polymer

Space–charge due to SCLC in the bulk is[46,57]

$$q_{sc}(E_F) = e\int_{E_F} g_{sc}(E) f(E_F - E_{Fo})\, dE_{Fp}. \tag{A2}$$

After zero temperature approximation, the conductive polymer bulk DOS is[37,57]

$$g_{sc}(E_F) = \frac{C_{sc}}{e\,S\,L}, \tag{A3}$$

where the differential space–charge capacitance is

$$C_{sc} = \frac{\partial Q_{sc}}{\partial U_{sc}} = LS\frac{\partial q_{sc}}{\partial U_{sc}}. \tag{A4}$$

2. Interface electrolyte-conductive polymer

Recombination current density is[46,57]

$$j_{rec} = e\,[A]\int_E f(E, E_F) g_{ct}(E) k_{ct\ eff}(E) dE. \tag{A5}$$

After zero temperature approximation, the surface DOS is[46,57]

$$g_{ct}(E_F) = [eR_{ct}(E_F) S[A] k_{et\ eff}]^{-1}, \tag{A6}$$

where the differential charge-transfer resistance is

$$[R_{ct}(E_F)]^{-1} = S\frac{\partial j_{rec}}{\partial U}. \tag{A7}$$

We also have from Eqs. (A3) and (A6)

$$k_{et\,\mathrm{eff}}(E_F) = \frac{L}{R_{ct}(E_F)C_{sc}(E_F)\,[A]} = \frac{L}{\tau(E_F)[A]}. \qquad \text{(A8)}$$

Quantities used and their units are: $e = 1.63 \times 10^{-19}$ C, $\omega = 2\pi f$ (Hz) frequency, L (cm) sample thickness, S (cm^2) sample area, (A) (mol^{-1}) activity of electrolyte, j_{rec} (A cm^{-2}) recombination current density, $U(V)$ applied voltage, $U_{sc}(V)$ bulk voltage, g_{ct} (cm^{-3} eV^{-1}), g_{sc} (cm^{-3} eV^{-1}) polymer surface DOS, R_{ct} (Ω) differential charge-transfer resistance, C_{sc} (F) space–charge capacitance, Q_{sc} (C) space–charge, q_{sc} (C cm^{-3}) volume density of charge, $k_{et\ \mathrm{eff}}$ (cm^4 s^{-1}) the effective bimolecular electronic transfer rate, E_F (eV) Fermi energy, E_{Fo} (eV) steady-state Fermi energy, and $E_{Fp(n)}$ (eV) quasi-Fermi energy.

REFERENCES

[1]K. P. Goetu and O. D. Jurchescu, *Handbook of Organic Materials for Electronic and Photonic Devices* (Elsevier, 2019), pp. 453–487.
[2]Nobel prizes for chemistry: 1953 Hermann Staudinger—Germany: "Discoveries in the field of macromolecular chemistry"; 1963 Giulio Natta—Italy and Karl Ziegler—Germany: "Chemistry and technology of high polymeric materials"; 1974 Paul J. Flory—USA: "Physical chemistry of macromolecules"; 1996 Robert F. Curl, Jr.—USA: "For the discovery of fullerene"; 2000 Alan J. Heeger—USA, Alan G. MacDiarmid—USA, and Hideki Shirakawa—Japan: "For the discovery of conductive polymers"; and 1992 R. A. Marcus—USA: "For contributions to the theory of electron transfer reactions in chemical systems."
[3]Y. Shirota and H. Kageyama, *Handbook of Organic Materials for Electronic and Photonic Devices* (Elsevier, 2019), pp. 3–42.
[4]A. Kohler and H. Bässler, *Electronic Processes in Organic Semiconductor: An Introduction* (Wiley-VCH Verlag GmbH & Co. KGaA, 2015).
[5]*Handbook of Organic Materials for Electronic and Photonic Devices, Oksana Ostroverkhova*, 2nd ed. (Woodhead Publishing, Elsevier, Cambridge, 2019).
[6]Organic and Printed Electronics Association, *OE-A Roadmap for Organic and Printed Electronics*, 8th ed. (VDMA Verlag, 2020), White Paper, ISBN: 978-3-8163-0736-5.
[7]H. Bässler, Phys. Status. Solidi B **175**, 15–56 (1993).
[8]B. A. Gregg, Soft Matter **5**, 2985–2989 (2009).
[9]R. A. Street, Y. Yang, B. C. Thompson, and I. McCulloch, J. Phys. Chem. C **120**, 22169 (2016).
[10]R. A. Street and D. M. Davies, Appl. Phys. Lett. **102**, 043305 (2013).
[11]C. Deibel, D. Mack, J. Gorenflot, A. Scholl, S. Krause, F. Reinert, D. Rauh, and V. Dyakonov, Phys. Rev. B **81**, 085202 (2010).
[12]J. Bisquert, G. Garcia-Belmonte, and J. Garcıa-Canadas, J. Chem. Phys. **120**, 6726 (2004).
[13]V. S. Bagotsky, in *Fundamentals of Electrochemistry* (Wiley Interscience, New York, 2004), ISBN: 0-471-70058-4.
[14]J. A. Carr and S. Chaudhary, Energy Environ. Sci. **6**, 3414–3438 (2013).
[15]D. D. Macdonald, Electrochim. Acta **51**, 1376 (2006).
[16]E. Barsoukov and J. R. Macdonald, in *Impedance Spectroscopy*, 2nd ed. (Wiley & Sons, 2005), ISBN: 0-471-64749-7.
[17]W. Schmickler, "Electronic effects in the electric double layer," Chem. Rev. **96**, 3177–3200 (1996).
[18]M. Dunwell, Y. Yan, and B. Xu, Curr. Opin. Chem. Eng. **20**, 151–158 (2018).
[19]R. A. Marcus, J. Chem. Phys. **24**, 966 (1956); R. A. Marcus, Rev. Mod. Phys. **65**, 599 (1993).
[20]R. A. Marcus, J. Chem. Phys. **94**, 4152–4155 (1990).
[21]S. Gosavi and R. A. Marcus, J. Chem. Phys. B **104**, 2067–2072 (2000).
[22]Y. Q. Gao, Y. Georgievskii, and R. A. Marcus, J. Chem. Phys. **112**, 3358–3369 (2000).
[23]J. R. Miller, L. T. Calcaterra, and G. L. Closs, J. Am. Chem. Soc. **106**, 3047–3049 (1984).
[24]K. K. Cline, M. T. McDermott, and R. L. McCreery, J. Phys. Chem. **98**, 5314–5319 (1994).
[25]C. Schubert, J. T. Margraf, T. Clark, and D. M. Guldi, Chem. Soc. Rev. **44**, 988 (2015).
[26]A. L. Eckermann, D. J. Feld, J. A. Shaw, and T. J. Meade, Coord. Chem. Rev. **254**, 1769–1802 (2010).
[27]M. Rudolph and E. L. Ratcliff, Nat. Commun. **8**, 1048 (2017).
[28]K. Wijeratnea, U. Aila, R. Brookea, M. Vagina, X. Liub, M. Fahlmanb, and X. Crispina, Proc. Natl. Acad. Sci. U.S.A. **115**, 11899–11904 (2018).
[29]J. W. Ondersma and T. W. Hamann, J. Am. Chem. Soc. **133**, 8264 (2011).
[30]S. Volk, N. Yazdani, E. Sanusoglu, O. Yarema, M. Yarema, and V. Wood, J. Phys. Chem. Lett. **9**, 1384–1392 (2018).
[31]R. A. Marcus and N. Sutin, Biochim. Biophys. Acta Rev. Bioenergetics **811**, 265 (1985).
[32]E. Palecek and M. Bartosik, Chem. Rev. **112**, 3427–3481 (2012).
[33]W. Schmickler and E. Santos, *Interfacial Electrochemistry* (Oxford University Press, New York, 1996), ISBN: 978-0-19-508932-5.
[34]X. de Vries, P. Friederich, W. Wenzel, R. Coehoorn, and P. A. Bobbert, Phys. Rev. B **97**, 075203 (2018).
[35]N. S. Lewis and M. S. Wrighton, J. Phys. Chem. **88**, 2009–2017 (1984).
[36]J. R. Miller, J. V. Beitz, and R. K. Huddleston, J. Am. Chem. Soc. **106**, 5057–5068 (1984).
[37]V. Nadazdy, F. Schauer, and K. Gmucova, Appl. Phys. Lett. **105**, 142109 (2014); F. Schauer, V. Nadazdy, K. Gmucova, M. Weis, I. Kuritka, J. Rohovec, J. Tousek, J. Touskova, and S. Lanyi, Nanosci. Nanotechnol. Lett. **5**, 1–5 (2013).
[38]N. S. Lewis, J. Phys. Chem. B **102**, 4843 (1998).
[39]A. M. Fajardo and N. S. Lewis, J. Phys. Chem. B **101**, 11136 (1997).
[40]W. J. Royea, A. M. Fajardo, and N. S. Lewis, J. Phys. Chem. B **101**, 11152–11159 (1997).
[41]S. W. Feldberg and N. Sutin, Chem. Phys. **324**, 216–225 (2006).
[42]N. S. Lewis, Z. Phys. Chem. **212**, 161 (1999).
[43]K. E. Pomykal and Nathan S. Lewis, J. Phys. Chem. B **101**, 2476 (1997).
[44]A. I. Cooper, Adv. Mater. **21**, 1291–1295 (2009).
[45]W. R. Salaneck, S. Stafstrom, and J. L. Brédas, *Conjugated Polymer Surfaces and Interfaces: Electronic and Chemical Structure of Interfaces for Polymer Light Emitting Devices* (Cambridge University Press, 1996).
[46]F. Schauer, V. Nádaždy, and K. Gmucová, J. Appl. Phys. **123**, 161590 (2018).
[47]B. D. Paulsen and C. D. Frisbie, J. Phys. Chem. C **116**, 3132 (2012).
[48]M. A. Lampert and R. B. Schilling, *Semiconductors and Semimetals* (Elsevier, 1970), Vol. 6, p. 96.
[49]O. Zmeskal, F. Schauer, and S. Nespurek, J. Phys. C Solid State Phys. **18**, 1873 (1985).
[50]F. Schauer, R. Novotny, and V. Cech, Chem. Pap. **50**, 206 (1996).
[51]M. Ates, Prog. Org. Coat. **71**, 1–10 (2011).
[52]B. Pejcic and R. De Marco, Electrochim. Acta **51**, 6217–6229 (2006).
[53]J. E. B. Randles, Disc. Faraday Soc. **1**, 11–19 (1947).
[54]A. Karki, J. Vollbrecht, J. Vollbrecht, A. J. Gillett, F. Schauer, T.-Q. Nguyen *et al.*, Adv. Energy Mater. **10**, 2001203 (2020).
[55]F. Schauer, M. Tkáčová, V. Nadáždy, K. Gmucová, M. Ožvoldová, L. Tkáč, and J. Chlpík, Polym. Degrad. Stability **126**, 204–208 (2016).
[56]S. Athanasopoulos, F. Schauer, V. Nádaždy, M. Weiß, F.-J. Kahle, U. Scherf, H. Bässler, and A. Köhler, Adv. Energy Mater. **9**, 1900814 (2019).
[57]F. Schauer, V. Nádaždy, K. Gmucová, and T. Váry, J. Appl. Phys. **124**, 165702 (2018).